International Journal of Engineering & Technology, 7 (4) (2018) 5798-5805

International Journal of Engineering & Technology

Website: www.sciencepubco.com/index.php/IJET
doi: 10.14419/ijet.v7i4.27189
Research paper

Single phase bridgeless welding source with reduced semiconductor devices and improved power quality

Manoj Kumar [1] *, Sanjeev Singh [2]

[1] *Electrical and Instrumentation Engineering Department SLIET Longowal Punjab (India) 148106*
[2] *Electrical Engineering Department, MANIT Bhopal, MP (India) 462003*
**Corresponding author E-mail: toomanoj@gmail.com*

Abstract

This paper presents a single phase bridgeless (BL) converter-based welding source with reduced semiconductor devices with improvement power quality at AC mains. The proposed BL welding source consists of two stages configuration. In first stage configuration bridgeless boost converter operated in continuous conduction mode (CCM), to achieve power factor near unity and input source current THD_i less than 5%. In second stage isolated two switch forward converter (TSWFC) is used to drive welding load with high frequency step down transformer (HFT). HFT provide electrical isolation between input supply and welding load. Output current control with short circuit handling capability is also ensured to achieve smooth and strong welding. The removal of diode bridge rectifier in BL converter at the input side, results in conduction loss reduction, increased efficiency and better thermal stability as compared to other conventional power factor correction (PFC) rectifiers. The controller performance is simulated in MATLAB SIMULINK and realized on a hardware prototype for validation of proposed concepts. The obtained results are presented for demonstration of effectiveness of proposed concept.

Keywords: *Bridgeless Converter; Power Factor Correction; Two Switch Forward Converter; Arc Welding Source.*

1. Introduction

In the past several years the transformer arc welding source is used for welding application. The use of transformer in welding sets, specially step-down transformer is used to provide isolation and increase the current so as to facilitate the easy melting of the welding rod. In transformer based welding has heavy and big size transformer, which makes it inconvenient to use in many of places such as high-rise buildings, house-hold uses. Further, the power quality of these welding sets at AC mains remains poor as it draws very heavy current in bursts. Application of high frequency in electrical transformers results in reduction of weight and volume. Therefore, some specific converters with controllers are required to maintain good power quality at AC mains along with controlled current to achieve good welding results.

Many efforts are being done to developed simple and robust power factor correction (PFC) topologies. Which actively adjust input current waveform to sinusoidal waveform. Generally a diode bridge rectifier is used as pre-regulator of PFC stage [1-2], this diode bridge rectifier is mainly responsible for conduction loss, poor system efficiency, higher thermal loss and big heat sink requirement for thermal stability. In bridgeless rectifier, less number of semiconductor switches are used in conduction path so that conduction loss is reduced. BL converter with modular configuration may be used for welding power source to increase the power rating of welding source [3].

High efficiency welding power source is in demand with additional features of light weight, robustness, safety, reliability, low cost and flexibility of operation. Moreover, sticking of the welding head must be avoided at any current level [4]. In order to meet all these requirements, it is important to ensure current regulation in a wide range. These needs are only met by incorporating high-frequency transformers fed by soft-switched inverters to the welding power Source [5-7]. Various publications reported in the literature on bridgeless ac-dc converter [3-4] and its benefits for various applications, however, little references are available for bridgeless single-phase welding source. This paper proposes a bridgeless single phase high frequency AC-DC converter based welding power source which has light weight, low volume, fast response, and fault tolerance, energy efficient operation and less semiconductor device used with improved power quality at AC mains [3] to complying with existing International Standard [8-9].

2. Proposed single phase bridgeless welding source

Circuit diagram of proposed single-phase Bridgeless (BL) welding source is shown in Fig.1. It consists of two-stage configuration; first stage configuration consists of a bridgeless power factor corrected AC-DC converter. It converts AC to regulated DC voltage and maintains the input power factor near unity. The proposed BL converter is created by joining two boost converters to operate sequentially in one half-cycle of the AC supply.

For positive half of AC inductor L_1, L_2 switch S_1, diode D_2' and D_1 carry the current to charge the dc-link capacitor C, whereas in negative half of AC inductor L_1, L_2, switch S_2, diode D_1' and D_2 carry the current. Continuous conduction of current is ensured through the input inductors L_1 and L_2 during the complete operation. An isolated two-switch forward converter (TWSFC) is used at second stage configuration for maintaining a constant output DC voltage and current for welding with current control feature. L_o is welding cable inductance.

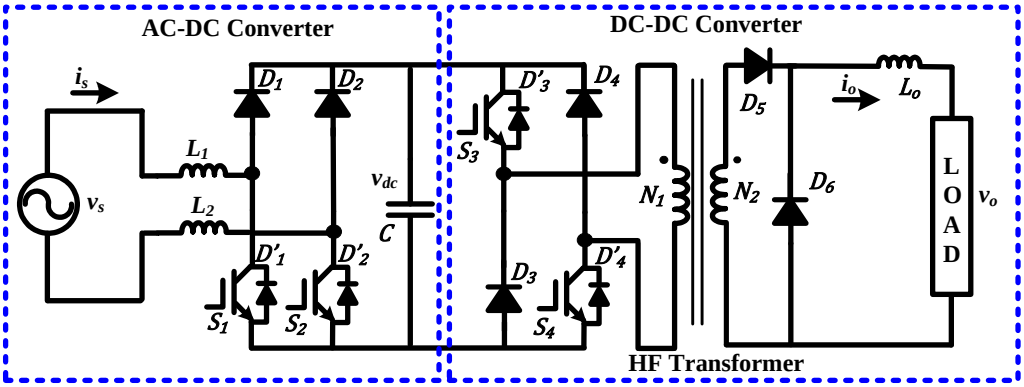

Fig. 1: Circuit Diagram of Single Phase Bridgeless Welding Source.

2.1. Operation of proposed single phase bridgeless converter

The proposed single-phase bridgeless welding source uses two boost converters operated sequentially, as first stage configuration and isolated two switch forward DC-DC converter, as second stage configuration. Fig.2 to Fig.5 presents the complete operation of the proposed converter in positive and negative cycles of the AC input supply.

The operation initiates with turning ON switch S_1, which applies the supply voltage v_s to input inductor L_1 and L_2 current through inductor increases. The current conduction takes place through diode D'_2 as shown in Fig.2. This is charging process of the boost inductor L_1 and L_2 .The stored energy in Inductor L_1 and L_2 is released to the dc-link capacitor C in next equivalent circuit shown in Fig.3, when the switch S_1 is turned OFF. The dc-link capacitor maintains constant current to load during charging of boost inductor (Fig.3). The operation in first half cycle replicates in the second half cycle with switch S_2, due to symmetrical topology of the converter, as shown in Fig.3 to Fig.4.

2.2. Mathematical model of proposed single phase bridgeless converter

The mathematical model of the single-phase bridgeless converter during positive half of ac voltage cycle is shown as equations (1) – (2). The current follows the path consisting of inductors , switch S_1 and diode D'_2, when the switch S_1 is on. During this period $(t_k < t < t_k + d_k T_s)$, the inductor stores energy whereas the capacitor dissipates the energy through the load.

$$v_s = L\frac{di_L}{dt} \tag{1}$$

$$C\frac{dv_{dc}}{dt} = -\frac{v_{dc}}{R_L} \tag{2}$$

During off state $(t_k + d_k T_s < t < t_{k+1})$ of switch S_1, the current flows through D_1, the parallel connected capacitor and load and D'_2.

$$v_s - v_{dc} = L\frac{di_L}{dt} \tag{3}$$

$$C\frac{dv_{dc}}{dt} = i_L - \frac{v_{dc}}{R_L} \tag{4}$$

The negative half of ac voltage cycle has equations similar to positive half cycle shown as Eq. (1) to (4). The mathematical models for the duration $(t_k < t < t_k + d_k T_s)$, and $(t_k + d_k T_s < t < t_{k+1})$ are shown as equations (5 - 6) respectively.

$$\begin{bmatrix} \frac{di_L}{dt} \\ \frac{dv_{dc}}{dt} \end{bmatrix} = \begin{bmatrix} \frac{1}{L} \\ 0 \end{bmatrix} v_s + \begin{bmatrix} 0 & 0 \\ 0 & -\frac{1}{R_L C} \end{bmatrix} \begin{bmatrix} i_L \\ v_{dc} \end{bmatrix} \tag{5}$$

$$\begin{bmatrix} \frac{di_L}{dt} \\ \frac{dv_{dc}}{dt} \end{bmatrix} = \begin{bmatrix} \frac{1}{L} \\ 0 \end{bmatrix} v_s + \begin{bmatrix} 0 & -\frac{1}{L} \\ \frac{1}{C} & -\frac{1}{R_L C} \end{bmatrix} \begin{bmatrix} i_L \\ v_{dc} \end{bmatrix} \tag{6}$$

Where $L = L_1 + L_2$, C, T_s and $R_L$are the input inductance, dc-link capacitance, switching period and DC-DC converter as a load, respectively. The modulation index $M = \frac{v_{dc}}{v_s} = \frac{1}{(1-d)}$ acts as voltage conversion ratio where d is ON time duty-cycle and $d' = (1 - d)$ represents OFF time duty cycle for input ac voltage v_s. From equations (5 - 6), the state matrices is represented as [10].

$$\bar{X} = \begin{bmatrix} i_L \\ v_{dc} \end{bmatrix}, \dot{X} = \begin{bmatrix} \frac{di_L}{dt} \\ \frac{dv_{dc}}{dt} \end{bmatrix} \tag{7}$$

$$\bar{A} = \begin{bmatrix} 0 & -\frac{1-d}{L} \\ \frac{1-d}{C} & -\frac{1}{R_L C} \end{bmatrix}, \bar{B} = \begin{bmatrix} \frac{1}{L} \\ 0 \end{bmatrix}, \bar{U} = [v_s] \tag{8}$$

$$\dot{X} = \bar{A}\bar{X} + \bar{B}\bar{U} \tag{9}$$

At steady state operation, the state variables of the bridgeless converter can be written as

$$\begin{bmatrix} \frac{di_L}{dt} \\ \frac{dv_{dc}}{dt} \end{bmatrix} = \begin{bmatrix} 0 & -\frac{1-d}{L} \\ \frac{1-d}{C} & -\frac{1}{R_L C} \end{bmatrix} \begin{bmatrix} i_L \\ v_{dc} \end{bmatrix} + \begin{bmatrix} \frac{1}{L} \\ 0 \end{bmatrix} [v_s] \tag{10}$$

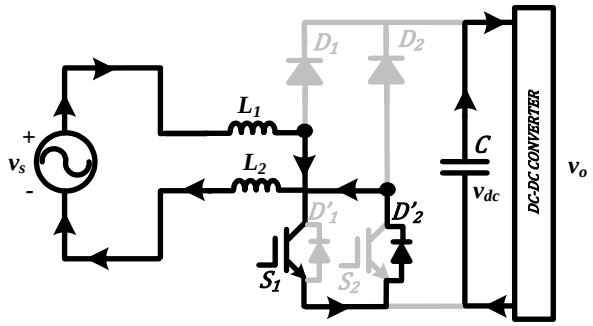

Fig. 2: Inductors Charging and C Discharging During AC Positive Cycle with S_1 Switch Turned ON.

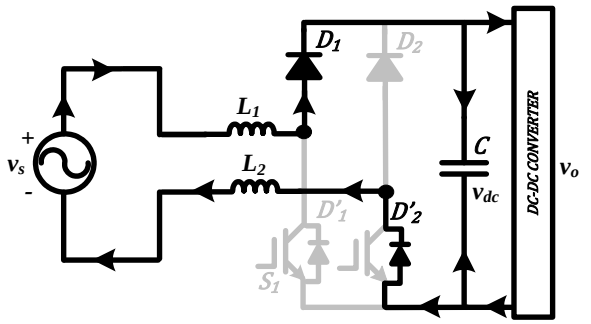

Fig. 3: Inductors Supply to C and Load during AC Positive Cycle with S_1 Switch Turned OFF.

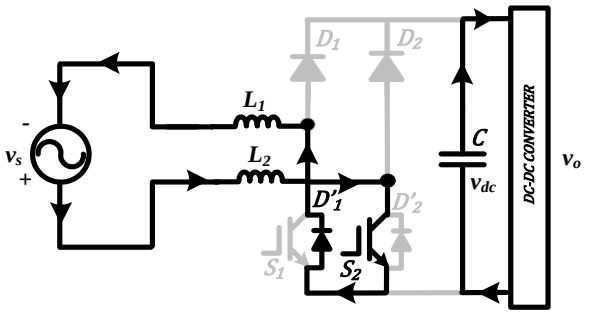

Fig. 4: Inductors Charging and C Discharging During AC Negative Cycle with S_2 Switch Turned ON.

2.3. Proposed average current control scheme

The BL boost converter control scheme, as shown in Fig.6, uses comparison of dc link voltage v_{dc} and reference voltage v_{dc}^* to generate voltage error v_e which is passed through a proportional-integral (PI) controller for control of power to maintain the desired dc-link voltage. AC input voltage template is used to generate the reference so that the input current i_s follows the sinusoidal shape of the v_s, however due to polluted v_s this task is sometimes impossible. Hence to remove this problem a PLL is used which generates a clean sinusoidal waveform with same frequency of input voltage v_s.

This voltage reference signal is multiplied with voltage error to generate a reference current i_s^*. This reference current i_s^* is compared with measured input current i_s to generate the current error. This error signal is fed to average current controller, where it is compared with high frequency triangular wave to generate switching pulses for switches S_1 and S_2.

This method uses the averaged value of inductor current for switching known as average current control using PI control [11]. The conventional PI control is represented by equations (11) and (12).

$$i^* = \frac{[(v_{dc}^* - v_{dc}).(K_{p1} + K_{i1}/S)].|v_s|}{V_m^2} \quad (11)$$

$$d = (i^* - |i_s|).\left(K_{p2} + \frac{K_{i2}}{S}\right) \quad (12)$$

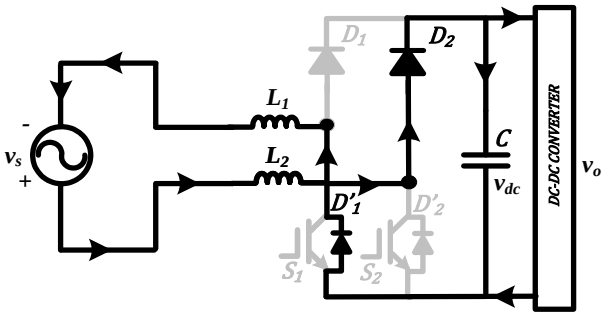

Fig. 5: Inductors Supply to C and Load during AC Negative Cycle with S_2 Switch OFF.

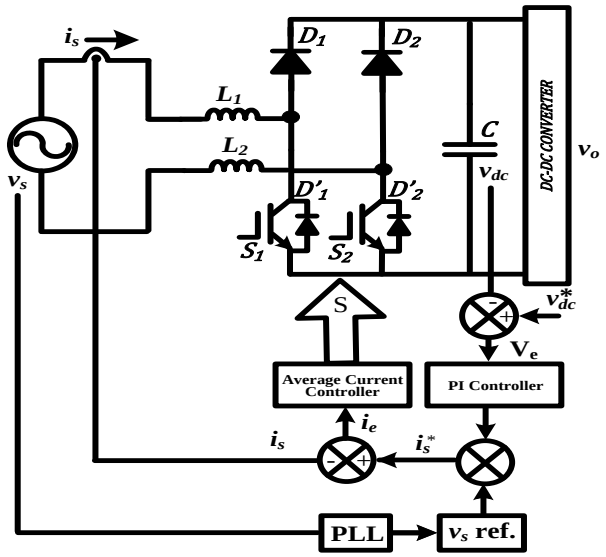

Fig. 6: Average Current Control Scheme for BL Boost Converter.

Where $(K_{p1} + K_{i1}/S)$ represents PI voltage controller and $\left(K_{p2} + \frac{K_{i2}}{S}\right)$ represents PI current controller. The control signal d is used to generate PWM pulses of constant frequency for the bridgeless PFC converter through its comparison with a sawtooth waveform. The Ziegler–Nichols method is used for obtaining gains K_p and $K_i$of PI controllers. In this method, initially, the integral gain K_i is set to zero and proportional gain, K_p is increased till the value (known as ultimate gain K_u) where the output starts oscillating with a constant amplitude. The oscillation period T_u along with K_u are used to decide the gains K_p and K_i as shown in Table 1. Here T_u is the oscillation frequency at the stability limit and K_u is the gain margin for loop stability [12]. Fig.6 shows the schematic diagram of the proposed PI control method for bridgeless PFC converter.

2.4. Operation of isolated two switch forward converter (TWSFC)

The two-switch forward converter is shown in Fig.7. The two-switch forward converter has two switches S_3 and S_4, and two clamp diodes D_3 and D_4. The switches are turn ON/OFF by applying current control switching pulse with maximum duty cycle of 0.5. The clamp diodes are used to recover magnetizing energy from the core which is stored during on time and it is fed back to the dc-link. The main objective of the clamping diodes are to reset the core of the transformer. The high frequency transformer (HFT) is used to step down the primary voltage and as well as to provide isolation between the input source and the output voltage v_o. The DC-DC converter output voltage v_o is given in equation (13) by neglecting the effect of parasitic element like resistance of inductor, ESR of capacitor.

Table 1: The Rules of Ziegler–Nichols Method

Control type	K_p	K_i	K_d
P	$\frac{K_u}{2}$	-	-
PI	$\frac{K_u}{2.2}$	$\frac{1.2K_p}{T_u}$	-
Classic PID	$0.6\ K_u$	$\frac{2K_p}{T_u}$	$\frac{K_p\ T_u}{8}$
Classic PID	$0.33\ K_u$	$\frac{2K_p}{T_u}$	$\frac{K_p\ T_u}{3}$
No Overshoot	$0.2\ K_u$	$\frac{2K_p}{T_u}$	$\frac{K_p\ T_u}{3}$

$$v_0 = D \times \left(\frac{N_2}{N_1}\right) \times v_{dc} \quad (13)$$

Where v_0 is DC-DC converter output voltage, n_2 is number of secondary turns of high frequency transformer, n_1 is number of

primary turns of HFT and v_{dc} is input dc-link voltage for DC-DC converter.

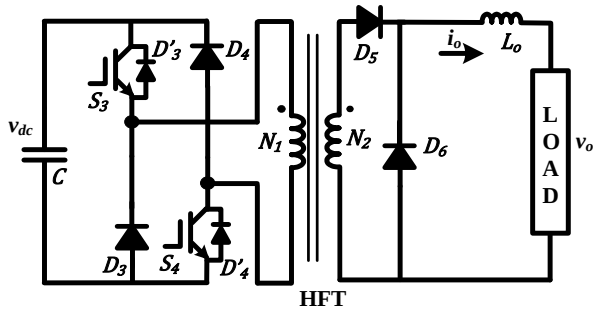

Fig. 7: Isolated Two Switches Forward DC-DC Converter.

During the steady state condition, the converter works in three modes of operation as discussed in the following section. The characteristic waveform of two switch forward converter is shown in Fig.8.

2.4.1. Mode1: Time interval $0 < t \leq DT_{sw}$

During the time interval of $0 < t \leq DT_{sw}$ the switches S_3 and $S_4$are turned on simultaneously and the dc-link voltage is applied across the primary of transformer and primary current starts builds up in the primary corresponding switching state shown in Fig.9. The turn's ratio times of input of v_{dc} is induced at the secondary of transformer, the diode D_5 is forward biased and load current also starts building up and increasing linearly. The relationship between voltage across primary and magnetizing current can be expressed as.

$$V_{pri} = v_{dc} - 2 \times v_{s3\ or\ s4} = L_m \times \frac{dI_m}{dt} \tag{14}$$

If neglecting voltage across the switches are minimal compared to DC link voltage and equation is expressed as

$$V_{pri} = v_{dc} = L_m \times \frac{dI_m}{dt} \tag{15}$$

Where, i_{s3} is current through the switch S_3, i_{s4} is current through the switch S_4, v_{s3} is voltage across the switch S_3, v_{s4} is voltage across the switch S_4, V_{pri} is voltage across the primary of HFT, L_m is the magnetizing inductance of HFT and $I_m$is the magnetizing current of HFT.

The voltage across the secondary of HFT is given as

$$V_{sec} = \left(\frac{N_2}{N_1}\right) \times v_{dc} \tag{16}$$

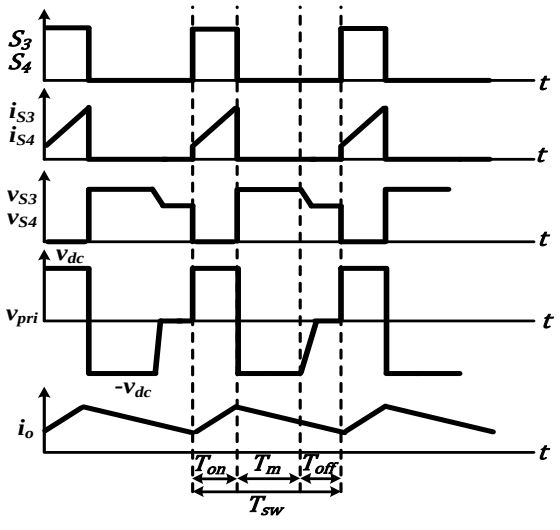

Fig. 8: Characteristic Waveform of Two Switch Forward DC-DC Converter.

The voltage across the output cable inductance v_{LC} is expressed as

$$v_{LC} = \left\{\left(\frac{N_2}{N_1}\right) \times v_{dc}\right\} - V_{D5on} - v_0 \tag{17}$$

The current through the output cable inductance is

$$i_L(t) = i_L(0) + \left[\frac{\left\{\left(\frac{N_2}{N_1}\right) \times v_{dc}\right\} - V_{D5on} - v_0}{L_o}\right] \times DT_{sw} \tag{18}$$

Where, $i_L(t)$ is the current through the output cable inductor L_o, $i_L(0)$ is the initial value of current through the output cable inductor, L_o is the output cable inductor and $T_{sw}$is the switching period of the DC-DC converter.

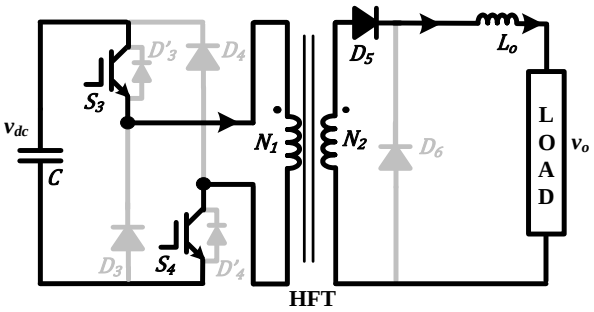

Fig. 9: Time Interval $0 < t \leq DT_{sw}$.

The current through transformer primary will be the sum of magnetizing current and turns ratio $\left(\frac{N_2}{N_1}\right)$ times the current through the cable inductance. The maximum duty cycle is restricted to 0.5 and this DC-DC converter will transfer energy from primary to secondary side during this interval only.

2.4.2. Mode2: Time interval $DT_{sw} < t \leq DT_{sw} + T_m$

When the switches S3 and S4 are simultaneously off for the time duration of DT_{sw} and the magnetizing current from the primary is fed back to the dc-link side through the clamp diodes D_3 and D_4, the corresponding switching state is shown in Fig.10. The diode D_5 is stop conducting, D_6 starts conducting and the voltage across the primary is negative of dc- link voltage value. In this interval, there was no power is transformed from primary side to secondary side. The relationship between voltage across the transformer primary and the magnetizing inductance is expressed as in equation (19)

$$-v_{dc} = L_m \times \frac{dI_m}{dt} \tag{19}$$

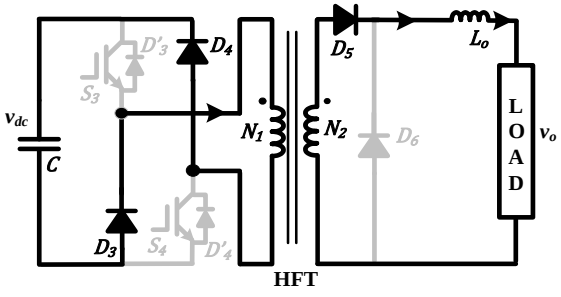

Fig. 10: Time Interval $DT_{sw} < t \leq DT_{sw} + T_m$.

2.4.3. Mode3: Time interval $DT_{sw} + T_m < t \leq T_{sw}$

In this interval, the switches S_3 and S_4 are off, the clamp diodes D_3, D_4 are off due to the reduction of magnetizing current to zero and output rectifier diode D_5 is reverse biased, the corresponding switching state is shown in Fig.11.

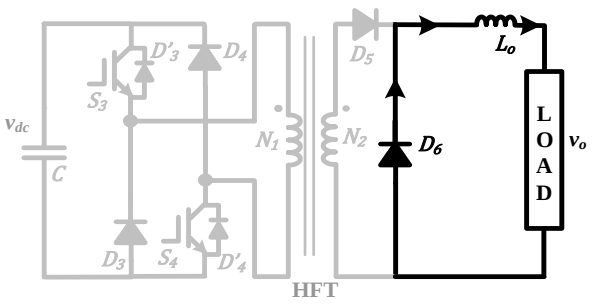

Fig. 11: Two Time Interval $DT_{sw} + T_m \ < t \leq \ T_{sw}$.

3. Simulation, experiential results and performance evaluation

In this section, the effectiveness of proposed single-phase bridgeless welding source is evaluated by simulating the proposed topology in MATLAB-Simulink environment. A prototype of the proposed bridgeless converter based circuit is fabricated in the laboratory. The controller is executed on a Texas instrument (TI) digital signal processor TMS320F2812 and the welding operation is carried out from single phase ac mains. Proposed bridgeless power source is developed in the Matlab-Simulink environment as shown in Fig.12.Table 2 shows the BL welding Source specifications.

Table 2: Single Phase BL Welding Source Specifications

System Specifications	
Input single phase voltage v_s	$220\pm20\%V_{ac}$
Welding Power P_o	$1kW$
Welding current i_o	$\leq 100Adc$
Switching frequency of ac to dc converter f_{s1}	$16kHz$
Switching frequency of dc-dc converter f_{s2}	$50kHz$
Open circuit Welding voltage $v_{o\ (open)}$	$80V$
Voltage $v_{o\ (short)}$	$10V$
Boost inductor L_1 and L_2	$500\mu H$
DC link Voltage v_{dc}	$400V$
Capacitor C	$1mF$
Welding cable Inductor L_o	$10\mu H$

Here the converter operates in the continuous conduction mode. The inductor value determines the amount of switching frequency ripple current which is linked with peak current flowing through the boost converter switch and rectifier. The low peak to peak ripple current minimizes the peak current flowing through power components (PFC switch and bridge rectifier). The minimum input voltage is considered for deriving worst case peak current via the power components. The high frequency ripple current also affects the size of input filter requirement and the input filter attenuates high frequency ripple produced by the boost converter. The current ripple depends on switching frequency and inductor value. In order to the reduce ripple current, the switching frequency and inductance value should be increased. Which means that by using higher switching frequency, the inductor size can be reduced and obviously the total power losses will increase and it requires more efficient heat sink structure. It will increase the size and cost. In most cases, efficiency, size, and noise are in a tradeoff relationship, requiring optimization. The switching frequency can be chosen as 16 kHz by considering the above facts. The inductor value of 1000μH is obtained with minimum rectified input voltage of $176Vac$, Nominal DC link boost voltage of 400 V_{dc} and the ripple current of 8A peak. The performance of the proposed Welding source is evaluated in different operating conditions to achieve unity power factor and minimized input current THD_i during welding operation.

Fig.13. shows the dynamic and steady state behavior of proposed single-phase BL welding source. Simulation results of Fig.13. show that at no load condition i.e. from t=0.1 sec. to t=0.2 sec and t=0.4 sec. to t=0.6 sec time a very small magnitude of current is drawn from input AC. However at t=0.2 sec to t=0.4 sec and t=0.6 sec time, when welding is started a high value of input AC current of approximately 8.2 A peak is drawn from AC supply.

Fig.14. shows the recorded experimental result of the laboratory prototype on a four channel digital storage oscilloscope (DSO). In Fig.14. Ch1 shows the input voltage v_s with 500V/div scale, Ch2 shows the input ac current i_s with 20A/div scale, Ch3 shows the dc link voltage v_{dc} with 400V/div scale and Ch4 shows welding current i_o with 100A/div scale.

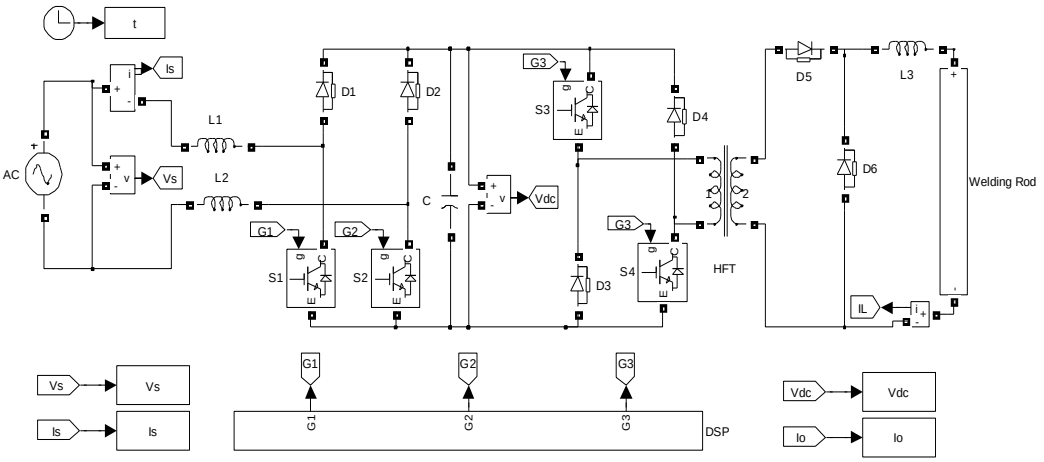

Fig. 12: MATLAB Simulation Model of Proposed Single-Phase BL Welding Source.

During no load condition a very low magnitude of input current i_s is drawn from input ac source and as the load is applied a high value of input ac current is drawn from input as shown in Fig.14. During entire welding process, the dc link voltage v_{dc} is constant and the load current is changed from zero to 100A.

Fig.15. shows the steady state behavior of proposed single-phase BL welding source. Simulation results of Fig.15. show that at welding load condition i.e. from t=0.22 sec. to t=0.4 sec time, when welding is started a high value of input AC current of approximately 8.2A peak is drawn from AC supply. Results show that constant current flow during welding time.

Fig.16. shows the recorded experimental result shows the input voltage v_s with 250V/div scale, Ch2 shows the input ac current i_s with 20A/div scale, Ch3 shows the dc link voltage v_{dc} with 400V/div scale and Ch4 shows welding current i_o with 100A/div scale. During welding condition, a constant magnitude 8.2 ampere peak input current i_s is drawn from input ac source and the welding current is constant as 100A.

During the entire welding process, the output DC link voltage of BL converter remains constant and the welding load current is zero at no load and 100 A at full load condition as depicted in the Fig. 13 to Fig.16.

Fig.17. to Fig.20. shows input current THD_i from no load to full load condition. During all time THD_i values remain less than 5%. It is seen from Fig. 13 to Fig.16 that from no load to full load condition the input AC current follows the input AC voltage waveform and the zero crossing of the two waveforms matches each other. This confirms the unity PF and very low value of $THD_i <$ 5% according to international power quality standard.

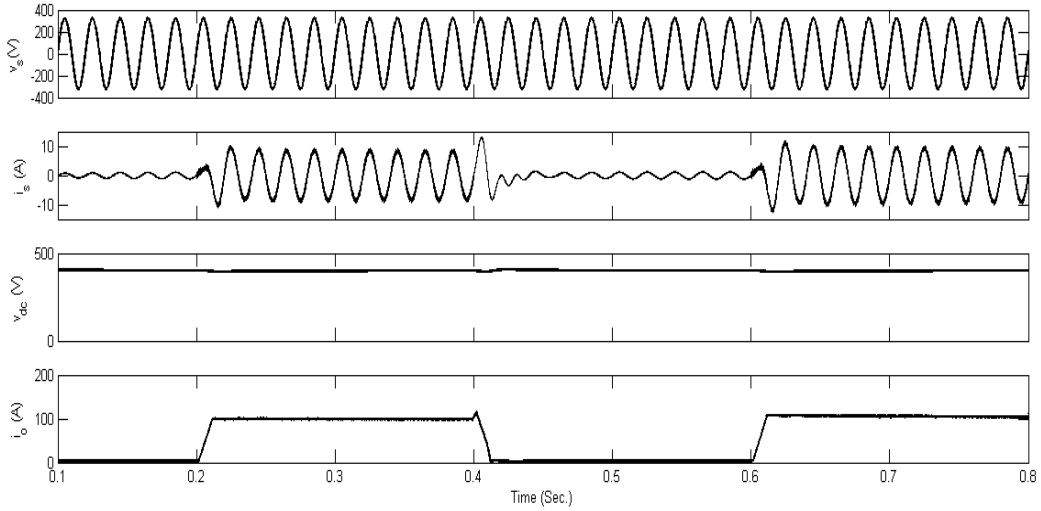

Fig. 13: Transient Performance Waveforms of v_s, i_s, v_{dc} and i_o (Simulated Result).

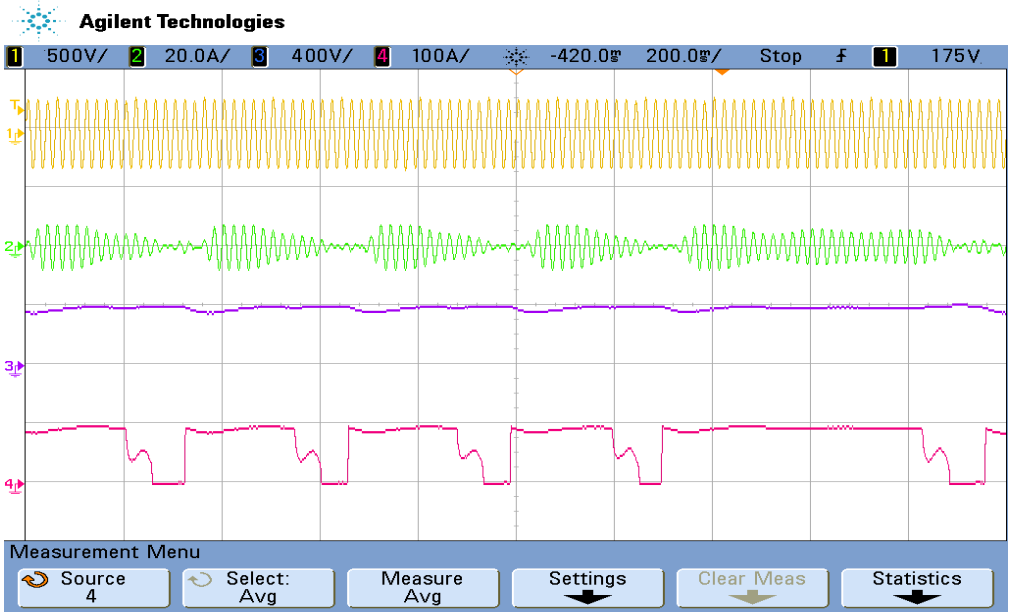

Fig. 14: Transient Performance Waveforms of v_s, i_s, v_{dc} and i_o(Practical Result).

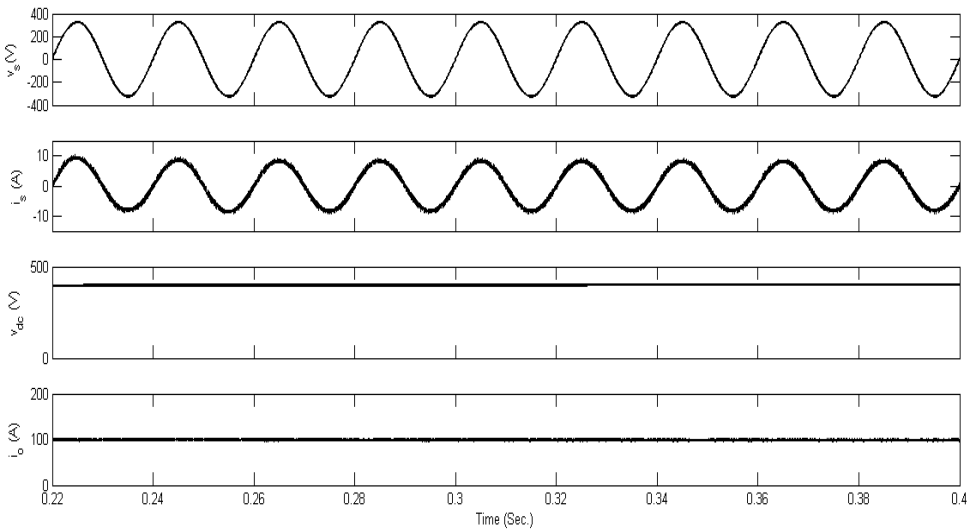

Fig. 15: Steady State Performance Waveforms of v_s, i_s, v_{dc} and i_o (Simulated Result).

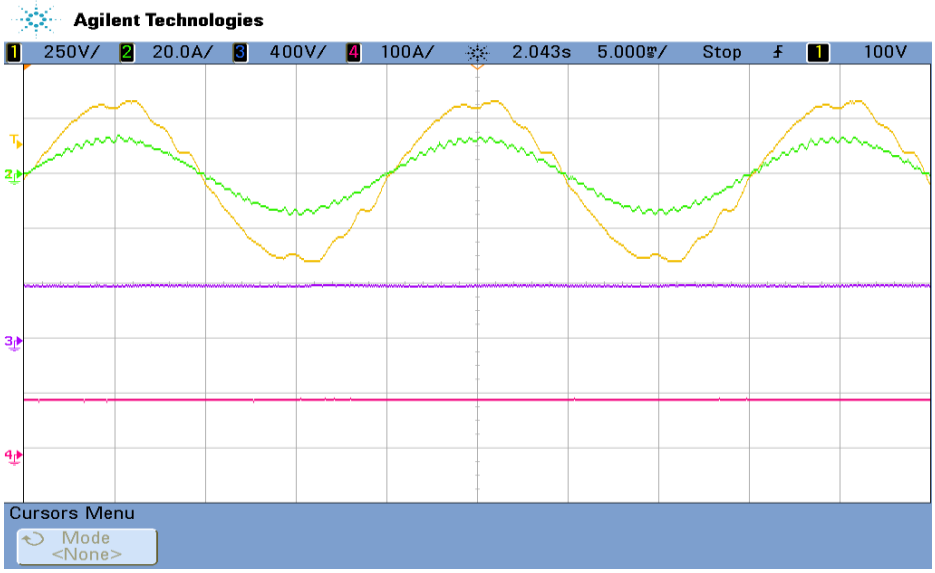

Fig. 16: Steady State Performance Waveforms of v_s, i_s, v_{dc} and i_o(Practical Result).

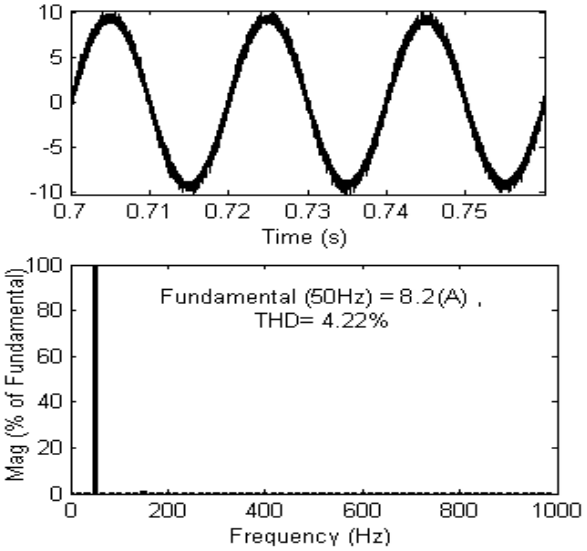

Fig. 17: Harmonics Spectrum of Input Ac Current during Welding (Simulated Result).

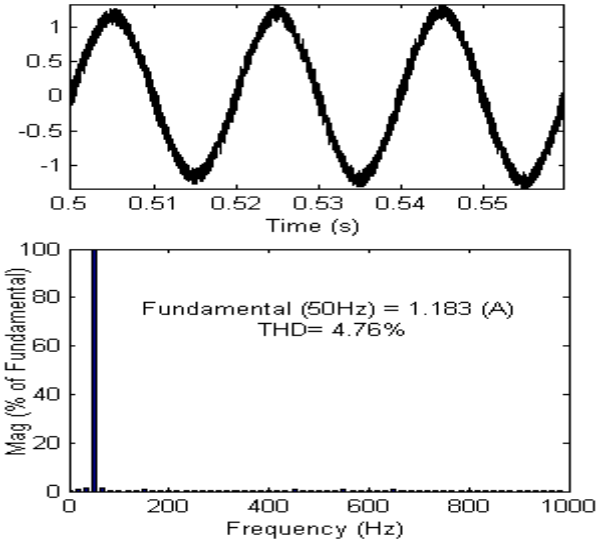

Fig. 19: Harmonics Spectrum of Input Ac Current before Starting Welding (Simulated Result).

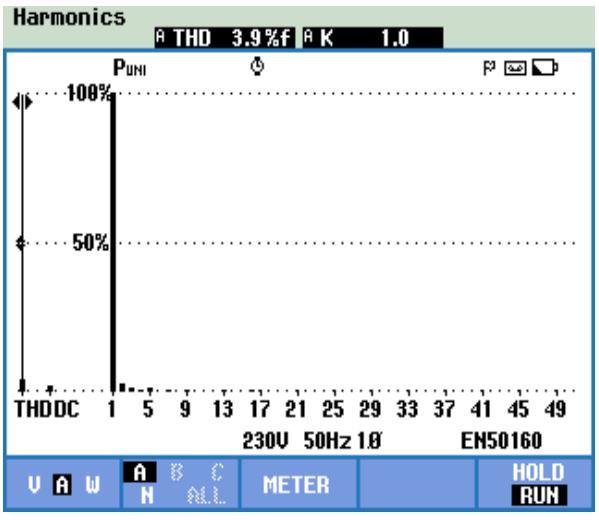

Fig. 18: Harmonics Spectrum of Input Ac Current during Welding (Practical Result).

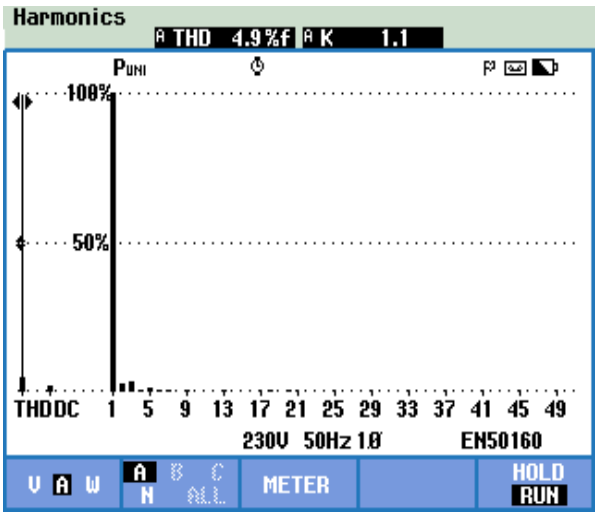

Fig. 20: Harmonics Spectrum of Input Ac Current before Starting Welding (Practical Result).

Fig.21 shows the power drawn from the ac input by the proposed BL converter based welding machine during welding process, i.e. 1kW at near unity (0.99) power factor.

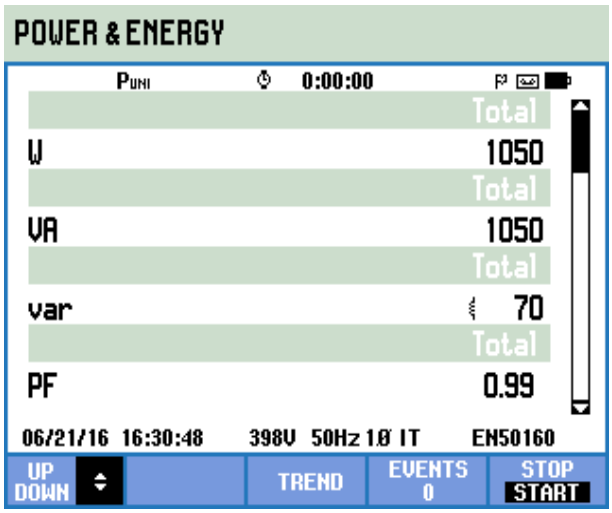

Fig. 21: Power and Power Factor during Welding (Practical Result).

4. Conclusion

A single-phase bridgeless converter based welding power source has been presented for improved power quality at AC mains, light weight and efficient operation with good quality of welding results. An exhaustive performance evaluation of proposed bridgeless converter welding supply has been carried out under varying load and AC mains voltage. From the presented performance results, it is concluded that the THD_i of the input AC mains current remains within 5% for rated load as well as light load conditions in a wide range of operating AC mains voltage.

References

[1] B. Singh, S. Singh, A. Chandra, & K. Al-Haddad, Comprehensive Study of Single-Phase AC-DC Power Factor Corrected Converters with High-Frequency Isolation, IEEE Transactions on Industrial Informatics, vol. 7, no. 4, (2011), pp. 540-556. https://doi.org/10.1109/TII.2011.2166798.

[2] J. C. Dias, & T. B. Lazzarin, A Family of Voltage-Multiplier Unidirectional Single-Phase Hybrid Boost PFC Rectifiers, IEEE Transactions on Industrial Electronics, vol. 65, no.1, (2018), pp. 232-241. https://doi.org/10.1109/TIE.2017.2721919.

[3] S. Narula, B. Singh, G. Bhuvaneswari & R. Pandey, Improved Power Quality Bridgeless Converter-Based SMPS for Arc Welding, IEEE Transactions on Industrial Electronics, 64(1), (2017), pp. 275-284. https://doi.org/10.1109/TIE.2016.2598519.

[4] E. H. Ismail, Bridgeless SEPIC Rectifier with Unity Power Factor and Reduced Conduction Losses, IEEE Transactions on Industrial Electronics, vol. 56, no. 4, (2009) pp. 1147–1157. https://doi.org/10.1109/TIE.2008.2007552.

[5] S.J. Jeon, G.H. Cho, Zero-voltage and zero-current switching full-bridge DC–DC converter for arc welding machines, Electron. Lett. vol. 35, issue. 13, Jun. 1999, pp. 1043-1044. https://doi.org/10.1109/TIE.2008.2007552.

[6] T. Madhulingam, T. Subbaiyan, P. Shanmugam, S. Kannan, Design and development of improved power quality based micro-butt-welding power supply, IET Power Electronics, vol. 10, issue.7, (2017),746-755. https://doi.org/10.1049/iet-pel.2016.0372.

[7] Y. Du, J. Wang, A.Q. Huang, Modeling of the High-Frequency Rectifier With 10-kV SiC JBS Diodes in High-Voltage Series Resonant Type DC–DC Converters, IEEE Transactions on Power Electronics, vol. 29, issue. 48 (Aug. 2014), pp. 4288-4300. https://doi.org/10.1049/iet-pel.2016.0372.

[8] International Standard IEC 61000-3-2, (2004). Limits for Harmonic Current Emissions (Equipment input current ≤16 A per phase.

[9] IEEE Guide for harmonic control and reactive compensation of Static Power Converters, IEEE Standard 519-1992.

[10] MH. Rashid, Power electronics handbook: devices, circuits, and applications, vol. 19. Academic Press, 2006, p. 525–30.

[11] A. Karaarslan, The Implementation of Bee Colony Optimization Algorithm to Sheppard–Taylor PFC Converter, IEEE Transactions on Industrial Electronics, 60(9), (2013), 3711–3719. https://doi.org/10.1109/TIE.2012.2204711.

[12] J.G. Ziegler, N.B. Nichols, Optimum settings for automatic controllers, Trans ASME (1942) 64:759-68.